RSC Advances

ROYAL SOCIETY OF CHEMISTRY

www.rsc.org/advances

Application of BSA-bioconjugated Phosphorescence nanohybrids into Protein detection in biofluids

Yanming Miao*

Shanxi Normal University, Linfen 041004, PR China

Short title: *Application of BSA-bioconjugated nanohybrids into Protein detection*

Category: *Biosensors*

* Corresponding author. Tel.: (86) 357-2051249; Fax.: (86) 357-2051243.
E-mail: mym8207@126.com.

Abstract: Since the major embodiment of biofunctions is protein, research on proteins is necessary before we can reveal the rules of life activities. However, because of the compositional complexity and high background fluorescence in biological samples, the bottleneck in protein research is how to selectively recognize the target proteins. Preparation of quantum dots (QDs) nanohybrids is an effective method for protein detection, and is very significant for development of QDs-based protein detection techniques. In this study, a cross-linking agent 1-ethyl-3-(3-dimethylaminopropy) carbodiimide/N-hydroxysuccinimide (EDC/NHS) was used to link QDs and bovine serum albumin (BSA) to form a nanohybrid BSA-Mn-ZnS Room-Temperature Phosphorescence (RTP) biosensor. Then this sensor was used into lysozyme detection. This study expands the application scope of nanohybrids in the field of life science. After the addition of lysozyme, there were strong electrostatic interaction and other interactions between BSA and lysozyme, which led to the inter-aggregation between BSA-Mn-ZnS and lysozyme and thereby enhanced RTP. Within a certain range, the enhancement of RTP is proportional to the dosage of lysozyme. On this basis, a high-performance sensor for lysozyme detection was built. This sensor can be used into lysozyme detection in biofluids. The detection limit of this sensor is 0.14 nM and the detection range is 0.4 - 40 nM.

Keywords: Lysozyme; Quantum dots; Nanohybrids

1 Introduction

With the implementation and promotion of human genome projects, life science research has entered the post-genomic era. The focus of life science research has transited from explanation of all life genetic information to investigation into biofunctions at the overall level. Since the major embodiment of bio-functions is protein, research on proteins is necessary before we can reveal the rules of life activities. Deep investigation into proteins will provide a material basis for research on rules of life activities, offers a theoretical basis and solutions for explaining and overcoming the mechanisms of many diseases, and is very significant for promotion of life science development. Many types of enzymes constitute a major part of protein research. Preparation of QDs nanohybrids is an effective route for protein detection, and is very significant for development of QDs-based protein detection techniques.

The QDs-protein composites that have been applied into biosensors are mostly based on the fluorescence of QDs.[1-3] As is well-known, the short-lived background fluorescence and scattered light from organisms will interfere with fluorescence detection. With longer lifetime compared with fluorescence, Room-Temperature Phosphorescence (RTP) QDs are more reliable and stable for molecular detection in biofluids, and this method is free from the interference of autofluorescence and scattering.[1, 4, 5] Phosphorescence is less frequent than fluorescence, which further improves the selectivity of RTP sensors.[6] Moreover, there is no need of complex pretreatment.[5, 7, 8] Owing to these advantages, RTP sensors have received higher attention from the research field and brought about some achievements.[4, 5, 8-15] If RTP

QDs were successfully applied into QDs-protein composites, the applications of nanomaterials into life science would be further expanded. At present, there are few reports about the application of biomacromolecule functionalized phosphorescent Mn-ZnS QDs as biosensors.

Lysozyme, also called muramidase or N-acetylmuramoylhydrolase, is an alkaline enzyme that can hydrolyze mucopolysaccharides (MPS) in pathogenic bacteria.[16] Lysozyme is a type of non-specific immune molecules ubiquitous in vivo and is also a major protein in saliva. Lysozyme can destroy the β-1,4 glucosidic bond between N-acetylmuramic acid and N-acetyl-D-(+)-glucosamine in cell walls, and thus decompose the insoluble MPS in cell walls into soluble glycopeptides, which lead to rupture of cell walls, leakage of contents and dissolution of bacteria. Especially in Gram-positive bacteria, lysozyme can selectively decompose cell walls without damaging other tissues. Thus, this non-toxic and harmless enzyme is a natural, safe and efficient disinfectant and antiseptic. In the field of medicine, urine lysozyme is used to detect lesions in renal tubules and glomeruli. Serum lysozyme detection is significant for identification of acute leukemia. Thus, lysozyme is widely used in protein research,[17-19] medical treatment[20, 21] and food industry.[22-24] There are many methods for lysozyme detection, such as turbidimetry,[25] microporous plate method,[26] enzyme-linked immunosorbent assay (ELISA),[18, 27] high-performance liquid chromatography,[28] fluorescence spectrophotometry,[29] fluorescence polarization,[30] and resonance light scattering (RLS).[15, 31] However, these methods are restricted by low sensitivity, operational complexity, high cost or low practicability. Thus, development

of a simpler, high-efficiency, low-cost and practical lysozyme detection method is very necessary.

In this study, a cross-linking agent 1-ethyl-3-(3-dimethylaminopropy) carbodiimide/ N-hydroxysuccinimide (EDC/NHS) was used to conjugate Mn-ZnS QDs and Bovine Serum Albumin (BSA) to form nanohybrids, which were then used into lysozyme detection. After the addition of lysozyme, there were strong electrostatic interaction and other interactions between BSA and lysozyme, which led to the inter-aggregation between BSA-Mn-ZnS and lysozyme and thereby enhanced RTP. Within a certain range, the enhancement of RTP is proportional to the dosage of lysozyme. On this basis, a high-performance sensor for lysozyme detection was built.

2. Experimental

2.1. Materials and Chemicals

MPA (J&K Scientific, Beijing, China), $Zn(Ac)_2 \cdot 2H_2O$, $Mn(Ac)_2 \cdot 4H_2O$, and $Na_2S \cdot 9H_2O$ (Tianjing Kermel Chemical Reagent Co., China) were used to prepare Mn-doped ZnS QDs. Ultrapure water (18.2 MΩ cm) was obtained from a Water Pro water purification system (Labconco Corporation, Kansas City, MO). 1-ethyl-3-(3-dimethylaminopropy)carbodiimide (EDC), N-hydroxysuccinimide (NHS) , Lysozyme and Bovine serum albumin (BSA) were provided by (J&K Scientific, Beijing, China).

2.2. Apparatuses

The morphology and microstructure of QDs were characterized by a JEM-2100 transmission electron microscope (TEM, Japan). The morphology and microstructure

of BSA-Mn-ZnS were characterized by a JSM-7500F scanning electron microscope (SEM, Japan). Phosphorescence was measured by a Cary Eclipse fluorescence spectrophotometer (Varian American Pty Ltd., America), equipped with a plotter unit and a quartz cell (1 cm × 1 cm) in the phosphorescence mode. pH was measured with a pH meter (Jinpeng Analytical Instruments Co. Ltd, China). The Resonance Light Scattering (RLS) spectra were recorded in the same spectrofluorometer by simultaneously scanning the excitation and emission monochromators ($\Delta\lambda = 0$) from 200 to 700 nm. Ultraviolet/visible (UV/Vis). Absorption spectra were measured by using a Shimadzu UV-29100 UV/Vis spectrophotometer.

2.3. Synthesis of Mn-Doped ZnS QDs

Mn-Doped ZnS QDs were synthesized in aqueous solution as per a published method[4, 5, 32] with minor modification. The specific steps are as follows: 5 mL of 0.1 M $Zn(Ac)_2$, 2 mL of 0.01 M $Mn(Ac)_2$, and 50 mL of 0.04 M MPA were added to a three-neck flask. The mixture was adjusted to pH 11 with 1 M NaOH. At room temperature under argon conditions, after 30 min of argon ventilation, then 5 mL of 0.1 M Na_2S was injected into the mixture. After stirring for 20 min, the solution was aged at 50 ℃ under open air for 2 h. The QDs were purified by precipitation with ethanol, centrifugation, washing with ethanol, and vacuum drying.

2.4 Bioconjugation between BSA and Mn-ZnS QDs

Bioconjugation between BSA and Mn-ZnS QDs was achieved via reported methods.[5, 33] Specifically, BSA was dissolved in a 10 mM phosphate buffer solution (PBS, pH 7.4) to form a 5.0 mg mL^{-1} solution, which was stored at 4 ℃. Then 5 mg of

Mn-ZnS QDs, 2 mg of EDC, and 1 mg of NHS were dissolved in 0.5 mL of PBS (10 mM, pH 7.4). The mixed solution was stirred at room temperature for ageing of 30 min, so that the carboxyl on surface of QDs would be fully activated. Then the above system was added with 0.5 mL of BSA, stirred at room temperature for 2 h, and then placed at 4 ℃ and in dark overnight, so that the unreacted EDC would be fully hydrolyzed. The BSA and Mn-ZnS QDs conjugated product was sent into membrane ultrafiltration, centrifugal separation, removal of unreacted BSA, followed by dissolution in 5 mL of 10 mM PBS (pH 7.4).

2.5. Detection methods

To investigate the effects of lysozyme on the RTP strength of BSA-Mn-ZnS nanohybrids, we dissolved lysozyme in water to form a 200 nM solution. To each of 10 mL colorimetric tubes, 0.25 mL of PBS (pH 7.4, 0.2 M) was added. Then the BSA-Mn-ZnS nanohybrids were dissolved in water to form a 1.0 mg mL^{-1} (as per mass of QDs) solution. This solution (100 μL, 20 mg L^{-1} computed as per mass of QDs) was added to each of the colorimetric tubes, followed by addition of different amounts of lysozyme (0 - 80 nM). After complete shaking and 10 min of standing, the tubes were sent to phosphorescence detection at the excitation wavelength at 295 nm.

2.6 Sample pretreatment

The urine sample was collected from healthy volunteer. Sample was subjected to a 100-fold dilution before analysis and no other pretreatments were used.

2.7 Sample detection

To the 5 ml colorimetric tubes, PBS (0.2 M, 0.25 mL), BSA-Mn-ZnS (1 mg

154 mL^{-1}, 100 μL) and urine (0.05 mL) were successively added. The mixed solutions
155 were diluted with ultrapure water and fully mixed, followed by 10 min of standing.
156 Then phosphorescence at excitation wavelength of 295 nm was determined. Each
157 experiment was repeated 3 times.

158 Spiked recovery experiments were used to validate the performance of this
159 sensor in lysozyme detection in biofluids. The spiked dosages were 5, 10 and 2.0 nM
160 lysozyme solutions. The urine was diluted 100 times without any other pretreatment.

161 **3. Results and analysis**

162 *3.1 Characteristics of MPA-capped Mn-doped ZnS QDs*

163 The shape and size of MPA-capped Mn-doped ZnS QDs were characterized with
164 transmission electron microscopy (TEM), and the size is about 3.5 nm (Fig. 2A). As
165 showed in Fig. 2B (SEM), the conjugation with BSA leads to aggregation (diameter
166 ~50 nm). On surface of QDs, the pK_{COOH} of MPA is 4.3 and the isoelectric point of
167 BSA is 4.7. In the pH 7.4 PBS, the QDs and BSA both are negatively charged, and
168 thus will not electrostatically interact to induce QDs aggregation. The possible reason
169 is that BSA binds the nearby QDs, and thus the SEM images exhibit aggregation
170 effect.[5]

171 As reported, Mn-doped ZnS QDs emit high phosphorescence, which is attributed
172 to the transition of Mn^{2+} $^4T_1$-$^6A_1$. After the excitation light is absorbed by ZnS matrix,
173 its electrons are stimulated. The holes as-formed will be captured by Mn^{2+}, while the
174 electrons and holes separately form composites with Mn^{2+}, which leads to the
175 excitation of Mn^{2+} and energy release in the form of phosphorescence, finally forming

an orange phosphorescent emission spectrum (about 590 nm).[34, 35]

Phosphorescence spectroscopy was used to characterize the conjugated product between Mn-ZnS QDs and BSA (Fig. 2C). The Mn-ZnS QDs emit a maximum excitation peak at 295 nm and leave a narrow concentrated emission band at 590 nm (Fig. 2C, a and b). After conjugation, the shapes of excitation and emission spectra do not change basically, but the intensity is slightly reduced (Fig. 2C, c and d). The bioconjugation may result in the formation of some defects on the surfaces of ZnS QDs, thereby slightly changing the excitation intensity. On the contrary, the luminescence center of Mn^{2+} which is in the ZnS crystal lattice is basically not impacted, and thus the position of emission spectrum does not change.

3.2. Mechanism of BSA-Mn-ZnS in lysozyme detection

Figure 3a shows the ultraviolet spectra of BSA-Mn-ZnS (curve 1), BSA-Mn-ZnS + lysozyme (curve b) and Mn-ZnS QDs (curve 3). After the conjugation of MPA-capped Mn-doped ZnS QDs and BSA, the ultraviolet spectra of BSA-Mn-ZnS are weakened and red-shift (curve 1). After lysozyme is added to BSA-Mn-ZnS, the ultraviolet spectra of BSA-Mn-ZnS + lysozyme are strengthened and red-shift (curve 2). These changes indicate that after QDs conjugate to BSA, the structure of QDs is changed, and significant interaction occurs between BSA-Mn-ZnS and lysozyme.

If two substances accumulate and produce scattering particles through electrostatic interaction, they will produce strong RLS signals. As showed in Fig. 3b, with the addition of lysozyme, the RLS of BSA-Mn-ZnS is gradually enhanced, indicating the aggregation of BSA-Mn-ZnS. The RLS of BSA-Mn-ZnS is gradually

198 weakened at wavelength 200-700 nm. However, with the increase of lysozyme
199 concentration, the RLS of BSA-Mn-ZnS is gradually enhanced, indicating that the
200 BSA-Mn-ZnS and lysozyme electrostatically interact to form nanohybrids. The
201 lysozyme can induce the aggregation of BSA-Mn-ZnS because of the special
202 compositions/ structures of BSA and lysozyme. The isoelectric points of BSA and
203 lysozyme are 4.7 and 11.0 respectively, and the PBS is at pH 7.4. Under these
204 conditions, BSA is negatively-charged on surface and the lysozyme is
205 positively-charged on surface. Thus, static electricity may be a key cause for the
206 aggregation between lysozyme and BSA-Mn-ZnS.

207 The TEM images (Fig. 2) of BSA-Mn-ZnS and the SEM images of
208 BSA-Mn-ZnS+lysozyme (Fig. 3c) indicate that after addition of 40 nM lysozyme into
209 the BSA-Mn-ZnS, the two substances will form larger aggregates.

210 Then very high concentration of NaCl was used to interfere with the RLS of the
211 BSA-Mn-ZnS lysozyme system. The results indicate that static electricity is the
212 major cause for the aggregation between lysozyme and BSA-Mn-ZnS (Fig. 3d), and
213 under 0.08 M ion intensity, the RLS of BSA-Mn-ZnS + lysozyme is significantly
214 reduced. With the increase of ion concentration, more cations are adsorbed onto the
215 surface of the negatively-charged QDs to neutralize the surface negative charge,
216 thereby inhibiting the electrostatic interaction between BSA-Mn-ZnS and lysozyme
217 and reducing the RLS intensity. Fig. 3e also shows that static electricity is a major
218 cause for the aggregation between BSA-Mn-ZnS and lysozyme. The RTP intensity
219 of the BSA-Mn-ZnS+lysozyme system is reduced with the increase of NaCl

concentration within 0.04-0.08 M. The increase of NaCl concentration inhibits the electrostatic interaction between BSA-Mn-ZnS and lysozyme, thereby quenching the RTP in the BSA-Mn-ZnS+lysozyme system.

However, when NaCl concentration > 0.1 M, the phosphorescence intensity of the BSA-Mn-ZnS + lysozyme system is enhanced and then unchanged (Fig. 3e), which indicates the presence of interaction in other structures, besides electrostatic interaction between BSA-Mn-ZnS and lysozyme.[36]

The results above indicate the presence of other interactions, besides the electrostatic interaction between BSA-Mn-ZnS and lysozyme. When the NaCl concentration is 0-0.04 M or > 0.08 M, the changes of NaCl concentration basically do not affect the system.

Analysis of absorption spectra is an efficient way for determination of structural changes in the protein molecules. The absorption spectra of BSA-Mn-ZnS and lysozyme (Fig. 4a) show that BSA-Mn-ZnS emits an ultraviolet absorption peak at 260 nm. With the addition of lysozyme, the absorption peaks of BSA-Mn-ZnS from 220 to 320 nm are enhanced, indicating the formation of light scattering particles between Mn-doped ZnS BSA-Mn-ZnS and lysozyme. With the ratio of 260nm/290nm absorptions (A_{260}/A_{290}) as Y-axis, and the concentration of enzyme as X-axis (Fig. 4b), then A_{260}/A_{290} is gradually reduced with the increase of lysozyme concentration, indicating that the addition of lysozyme will change the planar structure of BSA BSA-Mn-ZnS. These results also indicate the presence of other interactions, in addition to the electrostatic interaction between lysozyme and BSA-Mn-ZnS.

BSA-Mn-ZnS will aggregate under the interaction with lysozyme, which drives the BSA-Mn-ZnS closer. The electrons-holes-caused surface defects in QDs will produce a local electric field. With the addition of lysozyme, the mutual approach of BSA-Mn-ZnS QDs shortens the distance between BSA-Mn-ZnS QDs, which enhances the Coulomb force of Mn-doped ZnS QDs and leads to the enhancement of local electric field around the QDs. The enhancement of the local electric field will enable QDs to produce more effective excitation, so more energy will be transferred from the surface hole on QDs to Mn^{2+}, and enhance the RTP of Mn-doped ZnS QDs.[4, 37-39]

3.3 Molecular docking BSA and lysozyme

BSA-lysozyme docking was conducted to further reveal other BSA-lysozyme interactions, in addition to electrostatic interaction. Data about structures of BSA (PDB ID: 4F5S) and lysozyme (PDB ID: 2LYZ) were downloaded from Protein Data Bank (http://www.rcsb.org/). Then with BSA as a receptor protein and lysozyme as a ligand protein, the data were sent to ClusPro 2.0 protein-protein docking server (Structural Bioinformatics Laboratory of Boston University, http://cluspro.bu.edu/) for automatic molecular docking. Values of all parameters were default.

The docking results were classified into 29 Clusters, while the lowest energy in Cluster 0 was selected into analysis (Table 1). The docking results (Fig. 5a) show that the main interactions between BSA (green) and lysozyme (red) are hydrophobic interaction and hydrogen bonding. The amino-acid residues Ala568 or Pro572 from BSA can hydrophobically interact with the hydrophobic amino-acid residues Ala10 or

Leu129 from lysozyme. More importantly, double hydrogen bonding occurs between residues Asp562/Glu564 from BSA and Arg14 from lysozyme (Fig. 5b), and between residues Glu503 from BSA and Gly126/Cys127 from lysozyme (Fig. 5c). Moreover, hydrogen bonds are formed between residues Glu579 from BSA and Arg5 from lysozyme (Fig. 5d), and between residues Phe506 from BSA and Arg128 from lysozyme (Fig. 5e).

These results indicate that besides electrostatic interaction, the BSA-lysozyme interactions also include hydrophobic interaction and hydrogen bonding, which lead to the formation of stable composites not interfered with high ionic concentrations.

3.4 Effects of pH and ion concentration on the RTP of BSA-Mn-ZnS nanohybrids

The effects of various factors on the RTP intensity of BSA-Mn-ZnS nanohybrids were analyzed. Among these factors, pH is a major one. As showed in Fig. 6a, with the increase of pH within 4.5-7.5, the RTP intensity of BSA-Mn-ZnS nanohybrids is gradually enhanced and then maximized at pH 7.5. With the increase of pH within 7.5-9.0, the RTP intensity of BSA-Mn-ZnS nanohybrids is gradually reduced. The level of pH 7.4 in human body is set as the optimal pH of this sensor. The RTP intensity of BSA-Mn-ZnS nanohybrids is basically unchanged within 60 min (Fig. 6b).

3.5 Lysozyme detection based on RTP of BSA-Mn-ZnS nanohybrids

With the increase of lysozyme concentration, the RTP intensity of BSA-Mn-ZnS nanohybrids is gradually enhanced (Fig. 7a). On this basis, a lysozyme content detection sensor based on RTP of BSA-Mn-ZnS nanohybrids was built.

Under the optimal conditions, the changes of RTP intensity of BSA-Mn-ZnS nanohybrids (ΔRTP) and the lysozyme concentration are linearly correlated within certain ranges (Fig. 7b): the linear range is 0.4 - 40 nM and the linear equation is $\Delta RTP = 5.870\ C_{lysozyme} + 38.36$ (R = 0.994), with detection limit (3σ) 0.14 nM. For systems without addition of lysozyme and with addition of 2 nM lysozyme, the 11 continuous parallel detections on phosphorescence intensity have a relative standard deviation of 4.8%. The sensor is compared with other QDs-based methods (Table 2). Compared with the fluorescence RLS method and the fluorescence method,[15, 31, 40, 41] the new sensor avoids the interference from fluorescence and scattering in the biofluids and yields a lower detection limit.

3.6 Selectivity of the BSA-Mn-ZnS sensor

Some metal ions and biomolecules commonly present in biological fluids were selected to study the interference on the BSA-Mn-ZnS nanohybrids RTP sensor. With the presence of 10 nM lysozyme, the RTP intensity of the BSA-Mn-ZnS nanohybrids is not impacted by the addition of 4×10^6 fold Na^+, 1×10^6 fold K^+, 8×10^3 fold Ca^{2+}, 1.0×10^4 fold Mg^{2+}, 1.0×10^4 fold L-cysteine, 2×10^5 fold L-histidine, 2×10^5 fold L-glycin, or 20 mg L^{-1} human serum albumin.

3.7. Sample analysis

Fig. 8 indicates that the human urine and serum do not produce background phosphorescence (curve 1 and curve 2), but generate background fluorescence (curve 3 and curve 4). The reason is that the human fluids contain many proteins and biomolecules that can produce autofluorescence, but rarely generate

autophosphorescence. Therefore, this sensor is basically not interfered with the autofluorescence of biofluids, and is very suitable for lysozyme detection in biofluids.

The spiked recovery experiments further validate that the BSA-Mn-ZnS nanohybrids RTP sensor is feasible for lysozyme content detection in human fluids, with spiked recovery of 95% - 104% (Table 3).

4. Conclusions

In this study, a crosslinking agent EDC/NHS was used to conjugate QDs and BSA to form a BSA-Mn-ZnS RTP biosensor. Then this sensor was used into lysozyme detection. This study expands the application scope of nanohybrids in life science. After addition of lysozyme, there were strong electrostatic interaction and structural interaction between BSA-Mn-ZnS and lysozyme, which led to the inter-aggregation between BSA-Mn-ZnS and lysozyme and thereby enhanced RTP. Within a certain range, the enhancement of RTP is proportional to the dosage of lysozyme. On this basis, a high-performance sensor for lysozyme detection was built. This sensor can be used into lysozyme detection in biofluids. The detection limit of this sensor is 0.14 nM and the detection range is 0.4 - 40 nM. This sensor avoids the interferences from the autofluorescence and scattering in biofluids and outperforms other methods with a lower detection limit.

Acknowledgment

This work were supported by the Fund for Construction Program of Chemical Advantage and Key discipline of Shanxi Province of China (Grant 912019) and the Fund for research of School of Life Sciences of Shanxi Normal University (Grant SUYKZ-41).

330 **References**

331 1 J. M. Costa-Fernández, R. Pereiro, A. Sanz-Medel, *TrAC Trends in Analytical*
332 *Chemistry*, 2006, **25**, 207-218.

333 2 K. E. Sapsford, T. Pons, I. L. Medintz, H.Mattoussi, *Sensors*, 2006, **6**, 925-953.

334 3 R. Gill, M. Zayats, I. Willner, *Angewandte Chemie International Edition*, 2008, **47**,
335 7602-7625.

336 4 Y. He, H. F. Wang, X. P. Yan, *Chemistry-A European Journal*, 2009, **15**, 5436-5440.

337 5 P. Wu, Y. He, H. F. Wang, X. P. Yan, *Analytical chemistry*, 2010, **82**, 1427-1433.

338 6 J. M. Traviesa-Alvarez, I. Sánchez-Barragán, J. M. Costa-Fernández, R. Pereiro, A.
339 Sanz-Medel, *Analyst*, 2007, **132**, 218-223.

340 7 Y. He, H. F. Wang, X. P. Yan, *Analytical chemistry*, 2008, **80**, 3832-3837.

341 8 E. Sotelo-Gonzalez, M. T. Fernandez-Argüelles, J. M. Costa-Fernandez, *Analytica*
342 *chimica acta*, 2012, **712**, 120-126.

343 9 W. S. Zou, D. Sheng, X. Ge, J. Q. Qiao, H. Z. Lian, *Analytical chemistry*, 2010, **83**,
344 30-37.

345 10 H. B. Ren, X. P. Yan, *Talanta*, 2012, **97**, 16-22.

346 11 H. F. Wang, Y. Y. Wu, X. P. Yan, *Analytical chemistry*, 2013, **85**, 1920-1925.

347 12 Y. Miao, Z. Zhang, Y. Gong, Q. Zhang, G. Yan, *Biosensors Bioelectron*, 2014, **52**,
348 271-276.

349 13 Y. Miao, Z. Zhang, Y. Gong, Q. Zhang, G. Yan, *Biosensors Bioelectron*, 2014, **59**,
350 300-306.

351 14 P. Wu, J. Zhang, S. Wang, A. Zhu, X. Hou, *Chemistry – A European Journal*, 2014,

20, 952-956.

15 P. Wu, T. Zhao, Y. Tian, L.Wu, X. Hou, *Chemistry – A European Journal*, 2013, **19**, 7473-7479.

16 A. K. H. Cheng, B. Ge, H. Z. Yu, *Analytical Chemistry*, 2007, **79**, 5158-5164.

17 M. Buck, H. Schwalbe, C. M. Dobson, *Biochemistry-us*, 1995, **34**, 3219-3232.

18 M. L. Vidal, J. Gautron, Y. Nys, *J Agr Food Chem*, 2005, **53**, 2379-2385.

19 A. Ghosh, K. V. Brinda, S. Vishveshwara, *Biophys J*, 2007, **92**, 2523-2535.

20 O. M. Ogundele, *Mediat Inflamm*, 1998, **7**, 363-365.

21 S. Lee-Huang, P. Huang, Y. Sun, P. Huang, H. Kung, D. Blithe, H. Chen. *Proceedings of the National Academy of Sciences*, 1999, **96**, 2678-2681.

22 C. Z. Huang, K. A. Li , S. Y. Tong, *Analytica Chimica Acta*, 1997, **345**, 235-242.

23 L. Iucci, F. Patrignani, M. Vallicelli, M. E. Guerzoni, R. Lanciotti, *Food Control*, 2007, **18**, 558–565.

24 V. A. Proctor, F. E. Cunningham, D. Y. C. Fung, *C R C Critical Reviews in Food Science and Nutrition*, 2009, **26**, 359-395.

25 P. Mörsky, *Anal Biochem*, 1983, **128**, 77–85.

26 Y. C. Lee, D. Yang, *Anal Biochem*, 2002, **310**, 223-224.

27 N. Schneider, I. Weigel, K. Werkmeister, M. Pischetsrieder, *J. Agr. Food Chem* 2010, **58**, 76-81.

28 L. Pellegrino, A. Tirelli, *Int Dairy J.*, 2000, **10**, 435-442.

29 J. Chongqiu, L. Li, *Analytica Chimica Acta*, 2004, **511**, 11-16.

30 H. Miura, *Clin Biochem*, 1985, **18**, 40-47.

31 Z. Cai, H. Yu, M. Ma, *Spectrochimica Acta Part A: Molecular and Biomolecular Spectroscopy*, 2011, **78**, 1266-1271.

32 J. Zhuang, X. Zhang, G. Wang, D. Li, W. Yang, T. Li, *Journal of Materials Chemistry*, 2003, **13**, 1853-1857.

33 S. Wang, N. Mamedova, N. A. Kotov, W. Chen, J. Studer, *Nano Letters*, 2002, **2**, 817-822.

34 J. H. Chung, C. S. Ah, D. J. Jang, *The Journal of Physical Chemistry B*, 2001, **105**, 4128-4132.

35 R. Thakar, Y. Chen, P. T. Snee, *Nano letters*, 2007, **7**, 3429-3432.

36 N. K. Howell, N. A. Yeboah, D. F. V. Lewis, *Int J Food Sci Tech*, 1995, **30**,813-824.

37 O. Kulakovich, N. Strekal, A. Yaroshevich, S. Maskevich, S. Gaponenko, I. Nabiev, *Nano Letters*, 2002, **2**, 1449-1452.

38 P. Anger, P. Bharadwaj, *Physical review letters, 2006*, **96**, 113002.

39 Y. Hou, J. Ye, Z. Gui, G. Zhang, *Langmuir*, 2008, **24**, 9682-9685.

40 Y. Ying, Z. Zhentao, *Chinese. J. Anal. Chem.*, 2005, **33**, 650-652.

41 J. Li, X. W. He, Y. L. Wu, W. Y. Li, Y. K. Zhang, *Anal. Sci.*, 2007, **23**, 331-335.

Tables and Figures Captions

Table 1 BSA and lysozyme results of molecular docking scoring table.

Table 2 Comparison of the linear range and detection limit of several nanoparticles probes for the determination of lysozyme.

Table 3 Recovery for the determination of lysozyme in urine samples (Mean ± s; n = 3).

Fig. 1. Schematic illustration of fabrication of BSA-Mn-ZnS for lysozyme detection.

Fig. 2. (A) TEM image of MPA-capped Mn-doped ZnS QDs; (B) SEM images of BSA-Mn-doped ZnS QD bioconjugate; (C) The excitation (curves a, c) and RTP emission (cuwes b, d) spectra of Mn-doped ZnS QDs (20 mg L^{-1}; curves a, b), and the BSA-Mn-ZnS (20 mg L^{-1}; curves c, d). Inset: schematic illustration of electronic transition involved in the RTP emission from Mn-doped ZnS QDs. Solutions were prepared in PBS (10 mM, pH 7.4).

Fig. 3. (a) UV-vis absorption spectra of 1) BSA-Mn-ZnS, 2) BSA-Mn-ZnS+lysozyme, 3) the MPA-capped Mn-doped ZnS QDs; (b) Changes of BSA-Mn-ZnS RLS after addition of lysozyme; (c) SEM images of BSA-Mn-ZnS+lysozyme; (d) Changes of BSA-Mn-ZnS+lysozyme RLS after addition of NaCl; (e) Changes of BSA-Mn-ZnS+lysozyme RTP after addition of NaCl. Mn-doped ZnS QDs (20 mg L^{-1}), BSA-Mn-ZnS (20 mg L^{-1}), lysozyme (40 nM); Solutions were prepared in PBS (10 mM, pH 7.4).

Fig. 4. (a) The absorption spectra of BSA-Mn-ZnS in the presence of various concentrations of lysozyme; (b) The effect of the lysozyme concentration on A_{260}/A_{290}.

418 The concentration of BSA-Mn-ZnS is 20 mg L^{-1}.

419 **Fig. 5**. (a) Conjugation between BSA (green) and lysozyme (red); (b) double
420 hydrogen bonding of BSA Asp562 and Glu564 with lysozyme Arg14; (c) hydrogen
421 bonding betweeen BSA Glu579 and lysozyme Arg5; (d) double hydrogen bonding of
422 BSA Glu503 with lysozyme Gly126 and Cys127; (e) hydrogen bonding betweeen
423 BSA Phe506 and lysozyme Arg128.

424 **Fig. 6.** (a) Effect of pH on the RTP emission of the BSA-Mn-ZnS nanohybrids; (b)
425 Time-dependent RTP emission of the BSA-Mn-ZnS nanohybrids; The concentration
426 of BSA-Mn-ZnS are 20 mg L^{-1}; Slutions were prepared in PBS (10 mM, pH 7.4).

427 **Fig. 7.** (a) Lysozyme concentration-dependent RTP emission of the BSA-Mn-ZnS
428 nanohybrids; (b) Plots of ΔRTP as a function of lysozyme concentration show linear
429 range. Buffer, 10 mM PBS (pH 8.0); BSA-Mn-ZnS, 20 mg L^{-1}.

430 **Fig. 8.** The RTP and fluorescence spectra of urine (Curves 1, 3) and serum (Curves 2, 4).

431
432
433
434
435
436
437
438
439
440
441
442
443
444
445
446
447

448 **Table 1** BSA and lysozyme results of molecular docking scoring table.

Cluster	Members	Representative	Weighted Score	Cluster	Members	Representative	Weighted Score
0	156	Center	-682.8	14	19	Center	-738.9
		Lowest Energy	-685.5			Lowest Energy	-738.9
1	65	Center	-679.2	15	18	Center	-617.2
		Lowest Energy	-679.2			Lowest Energy	-659.1
2	64	Center	-634.0	16	17	Center	-602.4
		Lowest Energy	-636.1			Lowest Energy	-634.3
3	50	Center	-629.1	17	17	Center	-589.7
		Lowest Energy	-629.1			Lowest Energy	-608.6
4	50	Center	-619.6	18	16	Center	-719.8
		Lowest Energy	-698.9			Lowest Energy	-719.8
5	43	Center	-660.4	19	16	Center	-671.8
		Lowest Energy	-660.4			Lowest Energy	-671.8
6	41	Center	-690.0	20	14	Center	-660.4
		Lowest Energy	-690.0			Lowest Energy	-660.4
7	28	Center	-594.7	21	14	Center	-644.4
		Lowest Energy	-631.5			Lowest Energy	-644.4
8	27	Center	-618.7	22	12	Center	-629.2
		Lowest Energy	-642.6			Lowest Energy	-629.2
9	26	Center	-591.0	23	11	Center	-777.9
		Lowest Energy	-659.3			Lowest Energy	-777.9
10	26	Center	-645.3	24	11	Center	-655.5
		Lowest Energy	-645.3			Lowest Energy	-655.5
11	26	Center	-630.6	25	10	Center	-641.3
		Lowest Energy	-630.6			Lowest Energy	-641.3
12	23	Center	-621.6	26	10	Center	-623.6
		Lowest Energy	-621.6			Lowest Energy	-623.6
13	20	Center	-647.4	27	10	Center	-621.5
		Lowest Energy	-647.4			Lowest Energy	-621.5
14	19	Center	-738.9	28	10	Center	-605.0
		Lowest Energy	-738.9			Lowest Energy	-605.0

449

450 **Table 2** Comparison of the linear range and detection limit of several nanoparticles

451 probes for the determination of lysozyme.

Detection scheme	Linear range (nM)	LOD (nM)	Reference
Resonant Light Scattering (RLS) base on QDs	5.7–143	2.2	[31]
Resonant Light Scattering (RLS) base on QDs	4.3–286	0.68	[41]
Fluorescence base on QDs	36–2286	14	[40]
Resonant Light Scattering (RLS) base on QDs	10–100	3nM	[15]
Phosphorescence base on base on QDs	0.4–40	0.14 nM	This work

452

453

454

455

456

457

458

459

460

461

Table 3 Recovery for the determination of lysozyme in urine samples (Mean ± s; n = 3).

Type of samples	lysozyme spiked (nM)	Recovery (%)
Human urine	5	104 ± 5
	10	99 ± 5
	20	95 ± 4

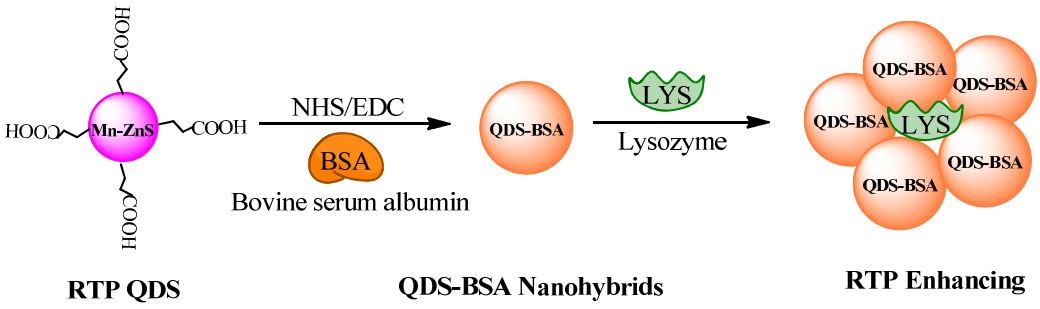

Fig. 1. Schematic illustration of fabrication of BSA-Mn-ZnS for lysozyme detection.

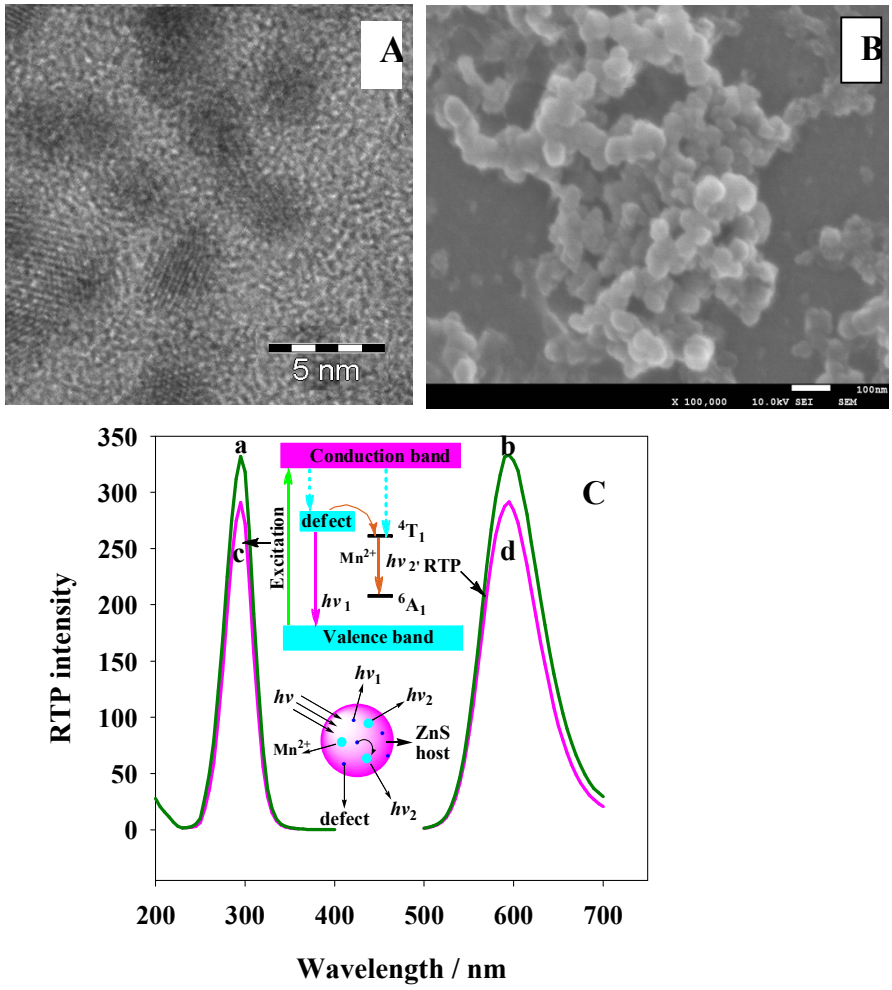

Fig. 2. (A) TEM image of MPA-capped Mn-doped ZnS QDs; (B) SEM images of BSA-Mn-doped ZnS QD bioconjugate; (C) The excitation (curves a, c) and RTP emission (cuwes b, d) spectra of Mn-doped ZnS QDs (20 mg L^{-1}; curves a, b), and the BSA-Mn-ZnS (20 mg L^{-1}; curves c, d). Inset: schematic illustration of electronic transition involved in the RTP emission from Mn-doped ZnS QDs. Solutions were prepared in PBS (10 mM, pH 7.4).

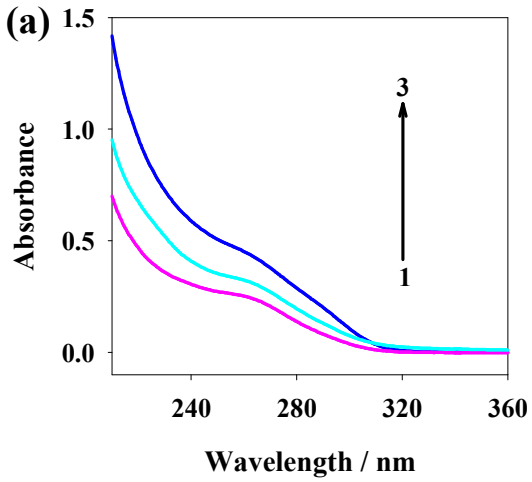

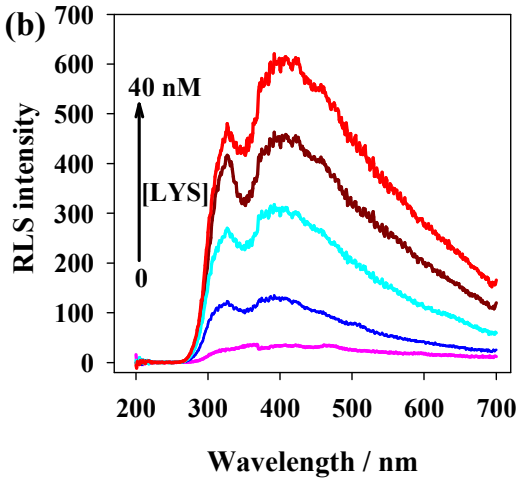

515

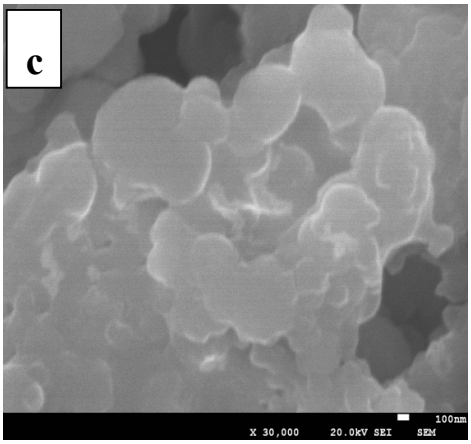

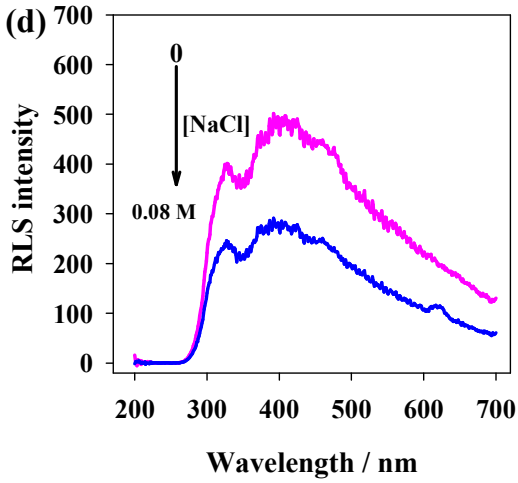

516

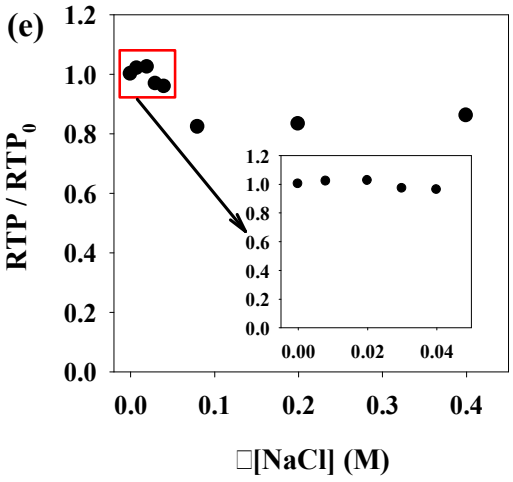

517

Fig. 3. (a) UV-vis absorption spectra of 1) BSA-Mn-ZnS, 2) BSA-Mn-ZnS+lysozyme, 3) the MPA-capped Mn-doped ZnS QDs; (b) Changes of BSA-Mn-ZnS RLS after addition of lysozyme; (c) SEM images of BSA-Mn-ZnS+lysozyme; (d) Changes of BSA-Mn-ZnS+lysozyme RLS after addition of NaCl; (e) Changes of BSA-Mn-ZnS+lysozyme RTP after addition of NaCl. Mn-doped ZnS QDs (20 mg L^{-1}), BSA-Mn-ZnS (20 mg L^{-1}), lysozyme (40 nM); Solutions were prepared in PBS (10 mM, pH 7.4).

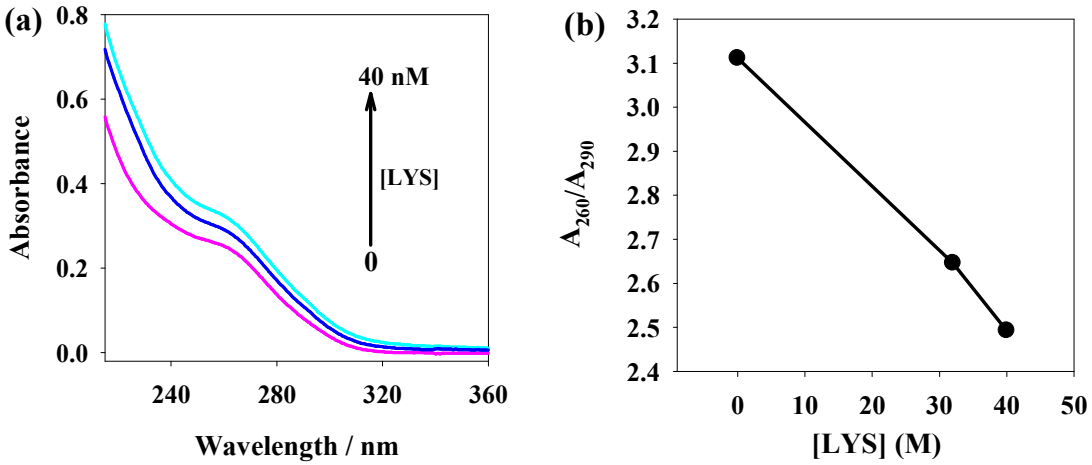

Fig. 4. (a) The absorption spectra of BSA-Mn-ZnS in the presence of various concentrations of lysozyme; (b) The effect of the lysozyme concentration on A_{260}/A_{290}. The concentration of BSA-Mn-ZnS is 20 mg L^{-1}.

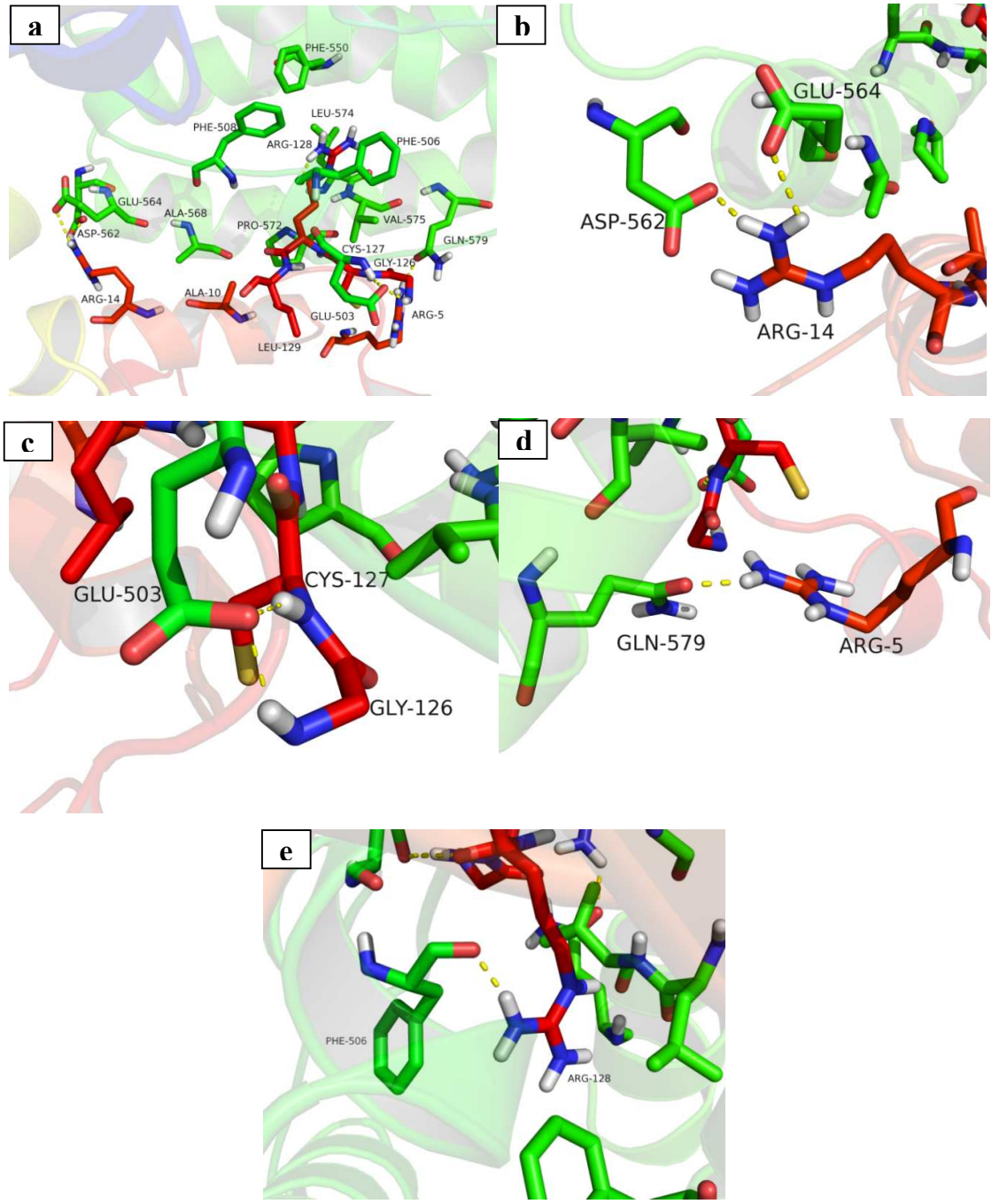

Fig. 5. (a) Conjugation between BSA (green) and lysozyme (red); (b) double hydrogen bonding of BSA Asp562 and Glu564 with lysozyme Arg14; (c) hydrogen bonding betweeen BSA Glu579 and lysozyme Arg5; (d) double hydrogen bonding of BSA Glu503 with lysozyme Gly126 and Cys127; (e) hydrogen bonding betweeen BSA Phe506 and lysozyme Arg128.

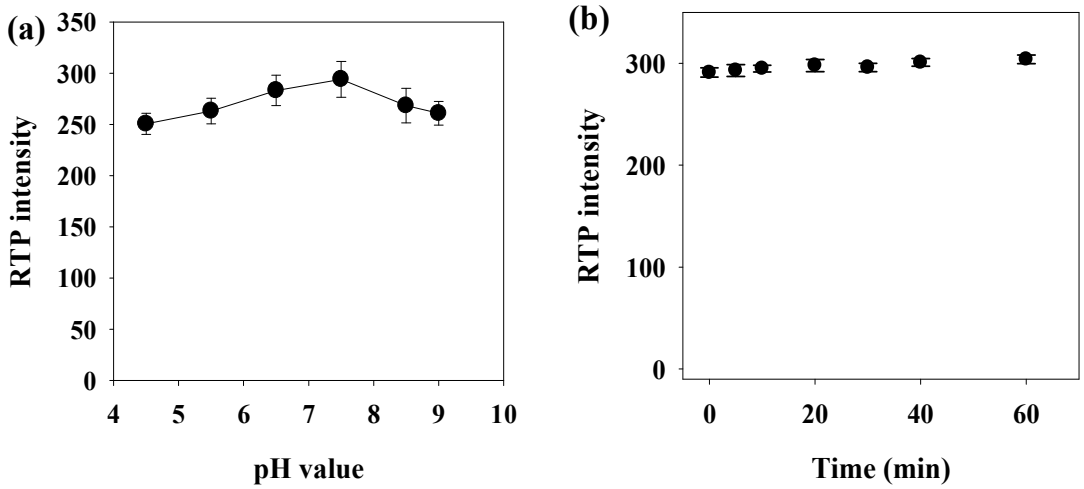

559

560 **Fig. 6.** (a) Effect of pH on the RTP emission of the BSA-Mn-ZnS nanohybrids; (b)
561 Time-dependent RTP emission of the BSA-Mn-ZnS nanohybrids; The concentration
562 of BSA-Mn-ZnS are 20 mg L^{-1}; Slutions were prepared in PBS (10 mM, pH 7.4).

563

564

565

566

567

568

569

570

571

572

573

574

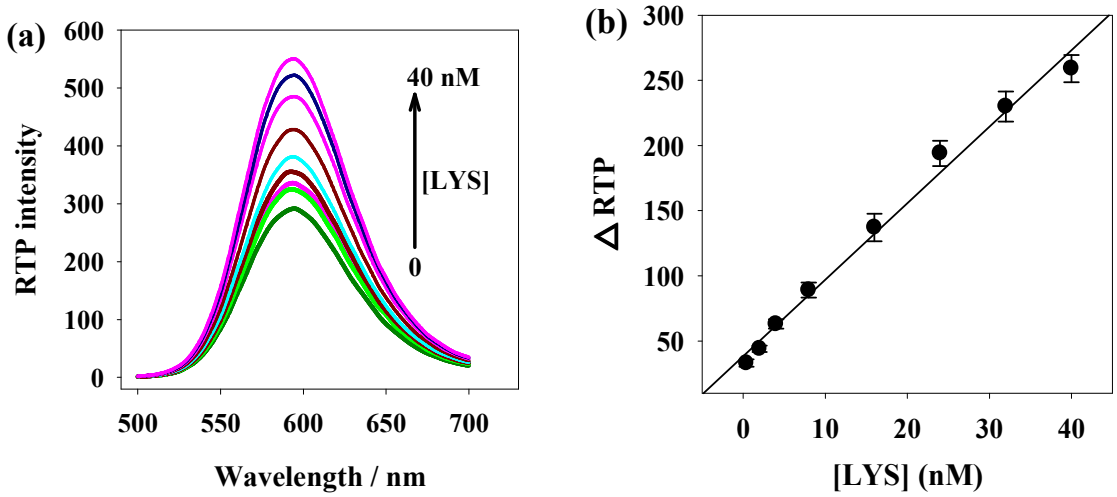

575

576 **Fig. 7.** (a) Lysozyme concentration-dependent RTP emission of the BSA-Mn-ZnS

577 nanohybrids; (b) Plots of ΔRTP as a function of lysozyme concentration show linear

578 range. Buffer, 10 mM PBS (pH 8.0); BSA-Mn-ZnS, 20 mg L^{-1}.

579

580

581

582

583

584

585

586

587

588

589

590

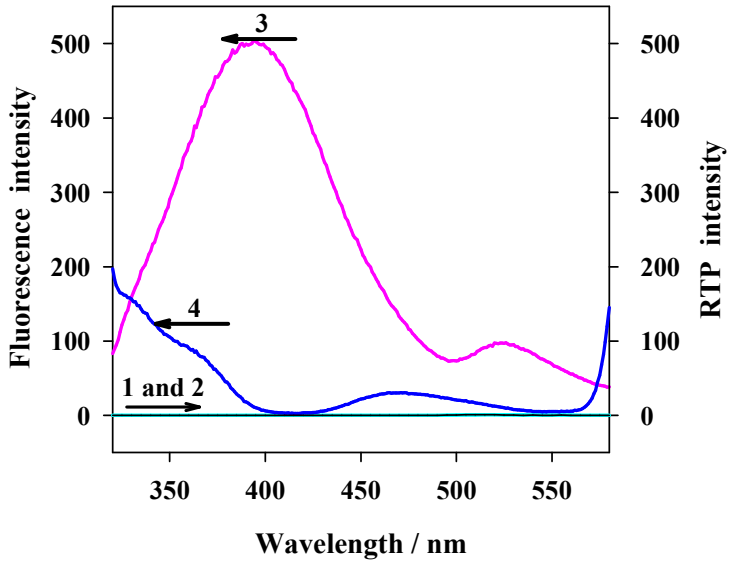

Fig. 8. The RTP and fluorescence spectra of urine (Curves 1, 3) and serum (Curves 2, 4).